Hydration of the Amylopectin Branch Point. Evidence of Restricted Conformational Diversity of the α-(1→6) Linkage

ARTICLE *in* JOURNAL OF THE AMERICAN CHEMICAL SOCIETY · OCTOBER 2004

Impact Factor: 12.11 · DOI: 10.1021/ja048622y · Source: PubMed

J|A|C|S
ARTICLES
Published on Web 09/15/2004

Hydration of the Amylopectin Branch Point. Evidence of Restricted Conformational Diversity of the α-(1→6) Linkage

Francisco Corzana,[†] Mohammed S. Motawia,[‡] Catherine Hervé du Penhoat,[§,⊥] Frans van den Berg,[†] Andreas Blennow,[‡] Serge Perez,[§] and Søren B. Engelsen*[,†]

Contribution from the Centre for Advanced Food Studies (LMC), The Royal Veterinary and Agricultural University (KVL), Rolighedsvej 30, DK-1958 Frederiksberg C, Denmark, Plant Biochemistry Laboratory, Department of Plant Biology and Center for Molecular Plant Physiology (PlaCe), The Royal Veterinary and Agricultural University (KVL), Thorvaldsensvej 40, DK-1871 Frederiksberg C, Denmark, and Centre de Recherches sur les Macromolécules Végétales, CNRS, BP 53X, 38041 Grenoble cédex, France

Received March 10, 2004; E-mail: se@kvl.dk

Abstract: The hydration behavior of a model compound for the amylopectin branch point, methyl 6′-α-maltosyl-α-maltotrioside, was investigated by combining molecular dynamics simulations in explicit water, 500 MHz NMR spectroscopy, including pulsed field gradient diffusion measurements, and exploratory multivariate data analysis. In comparison with results on a tetrasaccharide analogue, the study reveals that the conformational diversity of the three-bond α-(1→6) linkage becomes quite limited in aqueous solution upon the addition of a fifth glucose residue that elongates the α-(1→6) branch. This investigation reveals two plausible starch branch point structures, one that permits the formation of double helices and one that is adapted for interconnection of double helices. The apparent rigidity of the former is explained by the presence of water pockets/bridges in the vicinity of the branch point that lock the pentasaccharide structure into one conformational family that is able to accommodate the creation of the double-helical amylopectin structure.

Introduction

Starch is the primary energy reserve in higher plants and serves as the most important energy source in human food. This biodegradable polymer is a versatile renewable resource, and its potential has not yet been fully exploited. Starch is stored in the cells in granular form and is composed exclusively of glucose residues linked by only two types of glycosidic bonds, α-(1→4) and α-(1→6) glycosidic linkages. These components occur in two different macromolecular arrangements, amylose and amylopectin.[1] The former is essentially a linear α-(1→4)-D-glucan polymer, while amylopectin is a highly branched and slightly phosphorylated[2] macromolecule consisting of α-(1→4)-D-glucan short chains connected through α-(1→6) linkages. The short glucan chains are predominantly arranged in parallel oriented double-helical structures entwined at the nonreducing end.[3] Starch granules have diameters ranging from 0.1 to 200 μm, depending on the botanical source, and it is the assembly and packing of the amylopectin molecules that are responsible for the ordered semicrystalline granular structures formed during the deposition of starch in the plant. The α-(1→6) branch point is the key motif in the starch molecule, and it has been postulated that this branch point orients the glucan chains during starch granule biogenesis.

Diffraction and electron microscopy studies have revealed that the starch granule presents alternate crystalline and amorphous concentric layers with a 9−10 nm periodicity,[4] irrespective of the botanical source. The crystalline layers (4−7 nm thick) are attributed to the packing of amylopectin double-helical segments guided and most possibly stabilized by the α-(1→6) branch point configuration. While the branch point itself represents the limiting border between crystalline and amorphous domains in the amylopectin molecules, α-(1→6) linkages are also omnipresent in the amorphous lamellae[5] which have currently not been structurally characterized. The branched region of the starch granule has a crucial role in the molecular assembly of the starch granule.[6] Moreover, the lamella containing the α-(1→6) branch points determine the extent of granule hydration during the initial stage of starch granule gelatinization and subsequent swelling.[7] The detailed geometry and hydration of the starch branch point remains to be elucidated.

[†] Centre for Advanced Food Studies, The Royal Veterinary and Agricultural University.
[‡] Plant Biochemistry Laboratory, The Royal Veterinary and Agricultural University.
[§] Centre de Recherches sur les Macromolécules Végétales (affiliated with the University Joseph Fourier at Grenoble).
[⊥] Current address: Natural Sciences Complex, Department of Chemistry, University of Buffalo, State University of New York, Buffalo, NY 14260.

(1) Zobel, H. F. *Starch/Stärke* **1988**, *40*, 44−50.
(2) Blennow, A.; Engelsen, S. B.; Nielsen T. H.; Baunsgaard, L.; Mikkelsen, R. *Trends Plant Sci.* **2002**, *7*, 445−450.
(3) Imberty, A.; Chanzy, H.; Pérez, S.; Buléon, A.; Tran, V. H. *J. Mol. Biol.* **1988**, *201*, 365−378.
(4) Buléon, A.; Colonna, P.; Planchot, V.; Ball, S. *Int. J. Biol. Macromol.* **2001**, *23*, 85−112.
(5) Waigh, T. A.; Hopkinson, I.; Donald, A. M.; Butler, M. F.; Heidelbach, F.; Riekel, C. *Macromolecules* **1997**, *30*, 3813−3820.
(6) Blennow, A.; Hansen, M.; Schulz, A.; Jørgensen, K.; Donald, A. M.; Sanderson, J. *J. Struct. Biol.* **2003**, *143*, 229−241.

10.1021/ja048622y CCC: $27.50

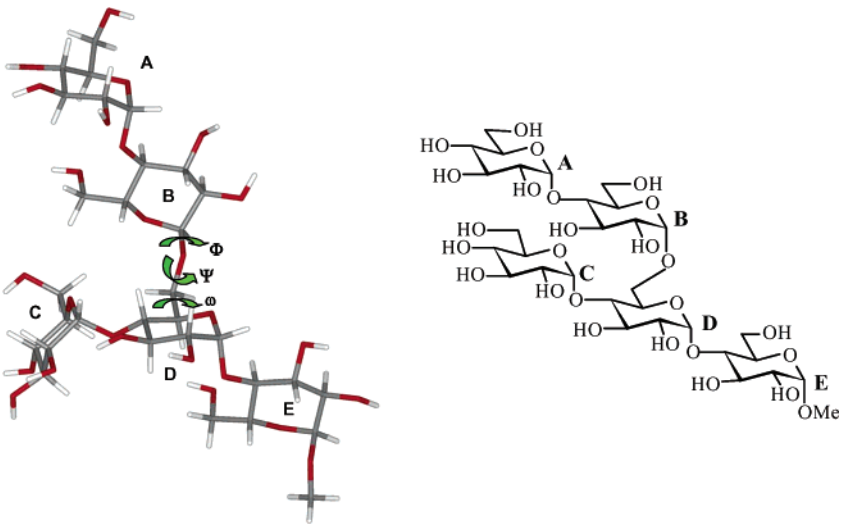

Figure 1. Molecular structure of the branched pentasaccharide. Residue labels and torsion angles of the branch point are indicated by characters used throughout the text.

Many observations suggest that carbohydrate structure and dynamics are significantly influenced by localized interactions with water.[8−11] While the magnitude of this influence on inherent properties remains debatable, it is clear that it is the nature of carbohydrate interactions with water that is responsible for many carbohydrate functionalities. For example, significant shifts are observed in the glass transition temperature for both amylose and amylopectin in the presence of water.[12]

To design new starch-based materials with well-defined properties, and to manufacture foods with desired functionalities, it is necessary to improve our understanding of carbohydrate−water interactions at the molecular level with special focus on the relationship between the hydration of starch (carbohydrate) structure and its functionality.[13]

For this reason, we have investigated the detailed hydration of the starch branch point using chemically synthesized methyl 6′-α-maltosyl-α-maltotrioside[14] (Figure 1) as a model compound. The same compound has recently been investigated as a primer for Starch Synthase II.[15] The study involves the use of NMR and molecular dynamics simulations in explicit water and is focused on the hydration of the branched pentasaccharide, with special emphasis on the influence of water on the preferred branching geometry. The molecular dynamics simulations were carried out using a second generation CHARMM-type force field[16] which provides a reasonably structured solute−water system and a significantly improved model of the α-(1→6) linkage. As a check on the validity of the simulations, homo- and heteronuclear coupling constants as well as translational and rotational coefficients were calculated from the trajectories and are compared to those determined by NMR measurements.

The number of molecular dynamics studies of the hydration of larger α-glucan fragments reported to date is rather limited and includes the study of the linear α-glucans maltohexaose[17] and maltodecaose.[18] In only one case has a branched tetrasaccharide (6″-α-D-glucopyranosyl-maltotriose) been characterized.[19] NMR investigations of branched α-glucans are limited to a few studies, all of which have been focused on chemical shift assignments and the structure of the solute.[19−21]

Methods

Nomenclature. Conformational flexibility around the α-(1→4) glycosidic linkages is described by two torsional angles, Φ = O5−C1−O1−C4′ and Ψ = C1−O1−C4′−C5′, and in the case of the α-(1→6) linkage by the three torsional angles, Φ = O5−C1−O1−C6′, Ψ = C1−O1−C6′−C5′, and ω = O1−C6′−C5′−O5′. The orientation of the hydroxymethyl groups is given by the torsional angle Θ = O5−C5−C6−O6, and the orientation of the methyl substituent at the reducing end of the pentasaccharide is given by the torsional angle Θ = O5−C1−O1−CMe. The orientations are also referred to by standard notation as either gauche−gauche (*gg*), gauche−trans (*gt*), or trans−gauche (*tg*), corresponding to Θ angles of 300°, 60°, and 180°, respectively. The sign of the torsion angles is defined in agreement with the IUPAC Commission of Biochemical Nomenclature.[22]

Synthesis. The strategy for the synthesis of the target molecule, methyl 6′-α-maltosyl-α-maltotrioside, was similar to the one previously described for the synthesis of 6′-α-maltosyl-maltotriose.[23] However, to obtain methyl 6′-α-maltosyl-α-maltotrioside, methyl 2,3,6-tri-*O*-benzyl-α-D-glucopyranoside[24−29] was used as the glycosyl acceptor instead of the glycosyl acceptor phenyl 2,3,6-tri-*O*-benzyl-1-thio-α-D-

(7) Jenkins, P. J.; Donald, A. M. *J. Appl. Polym. Sci.* **1997**, *66*, 225−232.
(8) Brady, J. W. *J. Am. Chem. Soc.* **1989**, *111*, 5155−5165.
(9) Engelsen, S. B.; Hervé du Penhoat, C.; Pérez, S. *J. Phys. Chem.* **1995**, *99*, 13334−13351.
(10) Kirschner, K. N.; Woods, R. J. *Proc. Natl. Acad. Sci. U.S.A.* **2001**, *98*, 10541−10545.
(11) Engelsen, S. B.; Monteiro, C.; Hervé du Penhoat, C.; Pérez, S. *Biophys. Chem.* **2001**, *93*, 103−127.
(12) Di Bari, M.; Cavatorta, F.; Deriu, A.; Albanese, G. *Biophys. J.* **2001**, *81*, 1190−1194.
(13) Franks, F. Hydration phenomena: an update and implications for the food processing industry. In *Water Relationships in Food*; Levine, H., Slade, L., Eds.; Plenum Press: New York, 1991; pp 1−19.
(14) Damager, I.; Olsen, C. E.; Møller, B. L.; Motawia, M. S. *Carbohydr. Res.* **1999**, *320*, 19−30.
(15) Damager, I.; Olsen, C. E.; Blennow, A.; Denyer, K.; Møller, B. L.; Motawia, M. S. *Carbohydr. Res.* **2003**, *338*, 189−197.
(16) Kuttel, M.; Brady, J. W.; Naidoo, K. J. *J. Comput. Chem.* **2002**, *23*, 1236−1243.
(17) Naidoo, K. J.; Kuttel, M. *J. Comput. Chem.* **2001**, *22*, 445−456.
(18) Momany, F. A.; Willett, J. L. *Biopolymers* **2002**, *63*, 99−110.
(19) Best, R. B.; Jackson, G. E.; Naidoo, K. J. *J. Phys. Chem. B* **2002**, *106*, 5091−5098.
(20) Bock, K.; Pedersen, H. *Carbohydr. Chem.* **1984**, *3*, 581−592.
(21) Jodelet, A.; Rigby, N. M.; Colquhoun, I. J. *Carbohydr. Res.* **1998**, *312*, 139−151.
(22) IUPAC−IUB. *Carbohydr. Res.* **1997**, *297*, 1−92.
(23) Motawia, M. S.; Olsen, C. E.; Enevoldsen, K.; Marcussen, J.; Møller, B. L. *Carbohydr. Res.* **1995**, *277*, 109−123.
(24) Bell, D. J.; Lorber, J. *J. Chem. Soc.* **1940**, 453−455.
(25) Petit, J. M.; Jacquinet, J. C.; Sinay, P. *Carbohydr. Res.* **1980**, *82*, 130−134.
(26) Garegg, P. J.; Hultberg, H. *Carbohydr. Res.* **1981**, *93*, C10−C11.

glucopyranoside. In this case, methyl *O*-(2,3,4,6-tetra-*O*-benzyl-α-D-glucopyranosyl)-(1→4)-*O*-(2,3,6-tri-*O*-benzyl-α-D-glucopyranosyl)-(1→6)-*O*-[(2,3,4,6-tetra-*O*-benzyl-α-D-glucopyranosyl-(1→4)]-*O*-(2,3-di-*O*-benzyl-α-D-glucopyranosyl)-(1→4)-2,3,6-tri-*O*-benzyl-α-D-glucopyranoside was obtained and debenzylated to provide the desired branched pentasaccharide, methyl 6′-α-maltosyl-α-maltotrioside.[15]

Nuclear Magnetic Resonance. The sample was lyophilized three times with D_2O (98.6%), and dissolved oxygen was vacuum-removed prior to sealing the sample in an NMR tube under argon. Complete sets of 2D NMR spectra were recorded on a 13 mM solution of methyl 6′-*O*-α-maltosyl-α-maltotrioside in 99.96% D_2O at both 5 and 25 °C. ^{1}H chemical shift assignments were obtained from phase-sensitive DQCOSY spectra, and carbon assignments were extracted from gHSQC and HMBC 2D spectra (Bruker Avance 500 and Varian INOVA 500 spectrometers). The digital resolution in the DQCOSY spectra was 0.4 Hz/pt. Selective proton-detected heteronuclear long-range 1D coupling constants were measured at 500 MHz on a Varian Unityplus spectrometer using a pulse sequence from the Varian library according to Blechta et al.[30] The digital resolution in the 1D spectra was 0.2 Hz/pt. The raw data were multiplied by an exponential line-broadening factor of 0.5 prior to applying the Fourier transform. Band-selective homonuclear decoupling was implemented during acquisition to simplify the antiphase multiplet that contained the $^3J_{C,H}$ values, thus increasing the accuracy of the data.

NOESY spectra were recorded at 5 and 25 °C with a mixing time of 400 ms. 1D DPFGSE-NOESY measurements described by Stott et al.[31] were acquired at 15 °C with selective pulses on the anomeric protons and a 400 ms mixing time. At room temperature, NOESY cross-peaks were not detected due to an unfavorable molecular tumbling time (τ_c). At lower temperatures (15 °C), the homonuclear NOEs were positive but very weak. Carbon heteronuclear NOEs (η_{CH}) were measured at 25 °C on a 100.6 MHz Bruker Avance 400 with a QNP probe with the inverse-gated pulse sequence. The η_{CH} values were obtained using the ratio of the integrals in the composite-pulse-decoupled and inverse-gated spectra (sensitivity-enhanced with line-broadening factors of 1.0 Hz). A rough estimate of the overall tumbling time was extracted from a plot of the reciprocal of the average methine η_{CH} value as a function of the theoretical spectral densities for a rigid rotor. Translational self-diffusion coefficients were obtained as previously reported[32] using the pulsed-field gradient stimulated spin−echo pulse sequence.[33]

Molecular Dynamics. Constant nVT Simulations Using CHARMM. Microcanonical molecular dynamics simulations were performed using the CHARMM program package[34] together with the CSFF[16] force field. The CSFF force field represents a second generation of the HGFB[35] force field. We also conducted full parallel simulations with the HGFB force field and obtained fairly similar results that will not be detailed here. It is noteworthy that the most ambitious characterization of the hydration of the amylopectin branching characteristics to date was performed on the tetrasaccharide 6″-α-D-glucopyranosyl-maltotriose using an intermediate generation carbohydrate force field that followed the HGFB but preceded the CSFF force field.[19]

The water molecules of the solvent were modeled using the TIP3P potential energy function.[36] In the simulation, Newton's equations of motion were integrated for each atom using the two-step velocity Verlet algorithm.[37] All hydrogen atoms were explicitly included in the simulations, although bond lengths involving hydrogen atoms were kept fixed throughout the simulation using the constraint algorithm SHAKE.[38] Minimum convention boundary conditions, a 1 fs time step, and a temperature of 300 K were used during the simulations. Interactions between atoms more than 12 Å apart were truncated, and switching functions were used to smoothly turn off long-range interactions between 10 and 11 Å. The list of nonbonded interactions was updated every 10 steps.

The coordinates of the starting conformation were superimposed upon the coordinates of a well-equilibrated box of 4096 water molecules (equilibrated at 300 K). This procedure left 4043 water molecules in the primary box after deleting those water molecules whose van der Waals radii overlapped with any of the atoms of the solute. After this virtual solvation, the system was energy minimized with 50 steepest descent iterations with the original box size in order to relax steric conflicts that might have been created during the generation of the box, and in order to relax the solute structure in the new environment. Next, the cubic box length was slightly adjusted to give a density of 1.00 g·cm^{-3}. Initial velocity for all atoms was assigned from a Boltzmann distribution at 300 K. The system was equilibrated for 100 ps to relax any artificial starting conditions induced by the solvation procedure, with occasional scaling of the atomic velocities when the average temperature deviated from the desired temperature of 300 K by more than an acceptance tolerance of ±3 K. Following this equilibration period, the Verlet integration was continued without any further interference for a subsequent 2 ns. Complete phase points were saved every 20 fs for analysis.

The molecular dynamics results are presented as normalized population density maps which are simple two-dimensional histogram representations of the trajectories in a two-torsional-angle space. For these calculations, the angular ranges of the dihedral angles are divided into 5° intervals for each histogram bin and divided by the total number of trajectory frames. For reasons of general comparison, the population density maps have been superimposed on the outer contours of the adiabatic maps of the maltose (8 kcal/mol) and isomaltoside (6 kcal/mol) calculated in the molecular mechanics program MM3.[39,40]

Exploratory Trajectory Analysis. Principal component analysis (PCA) is a powerful tool to explore large data sets[41] and was used to study the branched pentasaccharide dihedral simulation time profiles. The major dynamic flexibilities in the trajectories were investigated in a manner similar to that previously performed on DNA fragments.[42] Only the 44 heavy-atom dihedrals from the backbone structure were used in analysis. The dihedral trajectories contained 100 000 time frames of 20 fs, stacked in a data matrix **X** of the size 44 × 100 000. The *F*-component bilinear PCA model can be written as[41]

$$\mathbf{X} = \mathbf{t}_1 \cdot \mathbf{p}_1' + \mathbf{t}_2 \cdot \mathbf{p}_2' + ... + \mathbf{t}_F \cdot \mathbf{p}_F' + \mathbf{E} = \mathbf{T} \cdot \mathbf{P}' + \mathbf{E} \qquad (1)$$

$$\min_{\mathbf{T},\mathbf{P}} ||\mathbf{X} - \mathbf{T} \cdot \mathbf{P}'||^{2\prime}; \quad \mathbf{T}'\mathbf{T} = \mathbf{D} | d_1 \geq d_2 \geq ... \geq d_f; \quad \mathbf{P}'\mathbf{P} = \mathbf{I}$$

where $\mathbf{t}_f$ is a vector with 44 dihedral scores, $\mathbf{p}_f$ is a vector with 100 000 successive time frame loading values, **E** is the residual matrix or unmodeled part, **D** is a diagonal matrix with entries d_f sorted by size,

(27) Deninno, M. P.; Etienne, J. B.; Duplantier, K. C. *Tetrahedron Lett.* **1995**, *36*, 669−672.
(28) Debenham, S. D.; Toone, E. J. *Tetrahedron: Asymmetry* **2000**, *11*, 385−387.
(29) Elhalabi, J.; Rice, K. G. *Carbohydr. Res.* **2001**, *335*, 159−165.
(30) Blechta, V.; del Rio-Portilla, F.; Freeman, R. J. *Magn. Reson. Chem.* **1994**, *32*, 134−137.
(31) Stott, K.; Stonehouse, J.; Keeler, J.; Hwang, T. L.; Shaka, A. J. *J. Am. Chem. Soc.* **1995**, *117*, 4199−4200.
(32) Monteiro, C.; Hervé du Penhoat, C. *J. Phys. Chem. A* **2001**, *105*, 9827−9833.
(33) Tanner, J. E. *J. Chem. Phys.* **1970**, *52*, 2523−2526.
(34) Brooks, B. R.; Bruccoleri, R. E.; Olafson, B. D.; States, D. J.; Swaminathan, S.; Karplus, M. *J. Comput. Chem.* **1983**, *4*, 187−217.
(35) Ha, S. N.; Giammona, A.; Field, M.; Brady, J. W. *Carbohydr. Res.* **1988**, *180*, 207−221.
(36) Jorgensen, W. L.; Chandrasekhar, J.; Madura, J. D.; Impey, R. W.; Klein, M. L. *J. Chem. Phys.* **1983**, *79*, 926−935.
(37) Verlet, L. *Phys. Rev.* **1967**, *159*, 98−103.
(38) Ryckaert, J. P.; Ciccotti, G.; Berendsen, H. J. C. *J. Comput. Phys.* **1977**, *23*, 327−341.
(39) Allinger, N. L.; Rahman, M.; Lii, J.-H. *J. Am. Chem. Soc.* **1990**, *112*, 8293−8307.
(40) Corzana, F.; Motawia, M. S.; Hervé du Penhoat, C.; Pérez, S.; Tschampel, S. M.; Woods, R. J.; Engelsen, S. B. *J. Comput. Chem.* **2004**, *25*, 573−586.
(41) Jolliffe, I. T. *Principal Component Analysis*; Springer-Verlag: New York, 2002.
(42) Sherer, E. C.; Harris, S. A.; Soliva, R.; Orozco, M.; Laughton, C. A. *J. Am. Chem. Soc.* **1999**, *121*, 5981−5991.

and **I** is the identity matrix. Hence, the first component—dyad $\mathbf{t}_1 \cdot \mathbf{p}_1'$—gives the best least-squares rank-one approximation of the original matrix **X**, and the next component models the variation that remains after this rank-one approximation due to the orthogonality requirements. Successive components can thus be seen to capture common angular variation for all the 44 dihedrals, where dihedrals with a joined time profile will get a similar score value t_f. The sign of a $\mathbf{t}-\mathbf{p}$ couple is undetermined by eq 1.

The strength of PCA lies in the fact that large data tables often can be approximated well by only a few latent phenomena in the form of component pairs. By examining these components instead of the original variables, a simplified representation is obtained, suitable for exploratory diagnostics. The rank for **X** is bound by the number of rows and columns.[41] Therefore, in this application, we calculate a model on the covariance matrix **C** (size 44 × 44),

$$\mathbf{C} = (\mathbf{X}_m \cdot \mathbf{X}_m')/(n-1) = \mathbf{T} \cdot \mathbf{P}' + \mathbf{E} \qquad (2)$$

where $\mathbf{X}_m$ is the column mean-centered data matrix and n is the number of dihedrals. Due to the symmetry of **C**, **T** and **P** now differ only in magnitude. The dihedral scores **T** found in eq 2 are similar to the ones in eq 1. One component in eq 2 represents one common latent angular movement, and dihedrals with a relatively large score value t_f are interpreted as important for this latent movement, while a score value close to zero indicates less importance.

Calculation of Homo- and Heteronuclear Coupling Constants. In this work, ^3J coupling constants were calculated from the trajectories, utilizing the dependence of molecular dihedral structure on vicinal coupling constants through the Karplus relationship[43] by averaging over all frames in the trajectories. The heteronuclear coupling constants $^3J_{C,H}$ were calculated using the Karplus-type equation for the C−O−C−H segment parametrized by Tvaroska et al.,[44] and $^3J_{H,H}$ homonuclear coupling constants were calculated using the parametrization by Stenutz et al.[45]

Results and Discussion

Solute Geometry. Even for a relatively small molecule, such as the one studied here, equilibrium dynamics simulations in aqueous solution would require simulations longer than a millisecond which remain unrealistic today, and therefore we have adopted a Bayesian-like approach in which *a priori* information is utilized to cover as much as possible of the feasible conformational space. As our main focus was on the α-(1→6) branching linkage, we decided to run simulations initialized from three initial conformations, each corresponding to the different minima found in the adiabatic map of α-isomaltose.[46] One represents the same geometry of the α-(1→4) and α-(1→6) linkages that can be found in the crystal structure of α-panose[47] (($\Phi = 93°$, $\Psi = 229°$) and ($\Phi = 71°$, $\Psi = 165°$, $\omega = 76°$), respectively), and the two others have values for the ω-dihedral set to 300° and 180°. The trajectories initiated from each of these starting conformations will be denoted T1, T2, and T3, respectively. Since no transitions were observed for the dihedral angles of the α-(1→4) linkages, the procedure restricted the sampling of the conformational space of the glycosidic linkages to their predominant conformation. However, this choice would appear to be reasonable according to quantum mechanical and single-crystal X-ray evidence[48] as well as to intensive molecular dynamics studies on the disaccharide level.[40]

Prior to running molecular dynamics trajectories of the branched pentasaccharide in explicit water, a total vacuum trajectory of 20 ns was calculated. Figure 2 shows the population density maps obtained in a vacuum using the CSFF force field and starting conformations T1 and T2 (T1v and T2v). The vacuum trajectory initiated with T3 (T3v, not shown) gave the same results as those obtained from trajectory T1v. This starting conformation proved unstable in a vacuum, as the α-(1→6) linkage makes a rapid transition to the global ω-minimum of the branch point ($\omega = 60°$). Figure 2 reveals a tendency of the α-(1→4) linkages to adopt the same conformation as the one found in the crystal structure of α-maltose,[49] in which intramolecular hydrogen bonds between 1 O-2 and 2 O-3 are present, irrespective of the starting geometry. With respect to the α-(1→6) linkage, the major points of flexibility are the Φ and Ψ dihedrals, whereas transitions of the ω dihedral were not observed in the 20-ns total simulation time. The average values of the torsion angles Φ, Ψ, and ω in trajectories T1v and T2v are $\langle\Phi\rangle = 80°$, $\langle\Psi\rangle = 186°$, and $\langle\omega\rangle = 82°$ and $\langle\Phi\rangle = 76°$, $\langle\Psi\rangle = 113°$, and $\langle\omega\rangle = 285°$, respectively. In T1v, the α-(1→6) branch (D−B−A) adopts an antiparallel orientation with respect to the glucan backbone (E−D−C). In contrast, in trajectory T2v the α-(1→6) branch (D−B−A) adopts a parallel orientation as is found in amylopectin.

On the basis of these results, we decided to run molecular dynamic simulations on the branched pentasaccharide in explicit water starting only from conformations T1 and T2. Figure 3 displays the population density map of the glycosidic linkages calculated from the two trajectories. As previously observed for methyl α-maltoside,[40] when the second generation CSFF force field is used, there is a high preference in the trajectories for the α-(1→4) linkages to adopt the conformations centered around the minimum ($\Phi = 100°$, $\Psi = 220°$), which also encompasses the crystal structure of α-maltose.[49] The intramolecular hydrogen bond between O2(C) and O3(D) (distance O···O ≤ 3.3 Å) occurs about 48% of the time in trajectory T1, which is in good agreement with similar calculations reported for α-panose and for 6″-α-D-glucopyranosyl-maltotriose.[19]

The average conformations of the α-(1→6) branch point from the two trajectories are given in Table 1. In the T1 trajectory, no transitions in the Φ dihedral occurred, whereas relatively frequent transitions in the Ψ dihedral were observed. In this trajectory, two major conformations dominate, one with the Ψ dihedral close to 180°, which is populated about 58% of the time, and the other with Ψ around 90°. The Φ dihedral has a value close to 80° most of the time, in agreement with the exo-anomeric effect, and the average values of the torsion angles Φ, Ψ, and ω in the T1 trajectory are $\langle\Phi\rangle = 68°$, $\langle\Psi\rangle = 135°$, and $\langle\omega\rangle = 66°$. The geometry of the α-(1→6) branching is quite similar to the one proposed by O'Sullivan and Pérez[50] for the junction zone of two neighboring amylopectin double helices ($\Phi = 60°$, $\Psi = 180°$, and $\omega = 30°$) which yields an orthogonal branching that can interconnect two neighboring double helices (Starch "T1" in Table 1).

(43) Karplus, M. *J. Chem. Phys.* **1959**, *30*, 11−15.
(44) Tvaroska, I.; Hricovini, M.; Petrakova, E. *Carbohydr. Res.* **1989**, *189*, 359−362.
(45) Stenutz, R.; Carmichael, I.; Widmalm, G.; Serianni, A. S. *J. Org. Chem.* **2002**, *67*, 949−958.
(46) Dowd, M. K.; Reilly, P. J.; French, A. D. *Biopolymers* **1994**, *34*, 625−638.
(47) Imberty, A.; Pérez, S. *Carbohydr. Res.* **1988**, *181*, 41−55.
(48) French, A. D.; Kelterer, A. M.; Johnson, G. P.; Dowd, M. K.; Cramer, C. J. *J. Comput. Chem.* **2001**, *22*, 65−78.
(49) Takusagawa, F.; Jacobsen, R. A. *Acta Crystallogr., Sect. B: Struct. Sci.* **1978**, *34*, 213-218.
(50) O'Sullivan, A. C.; Pérez, S. *Biopolymers* **1999**, *50*, 381−390.

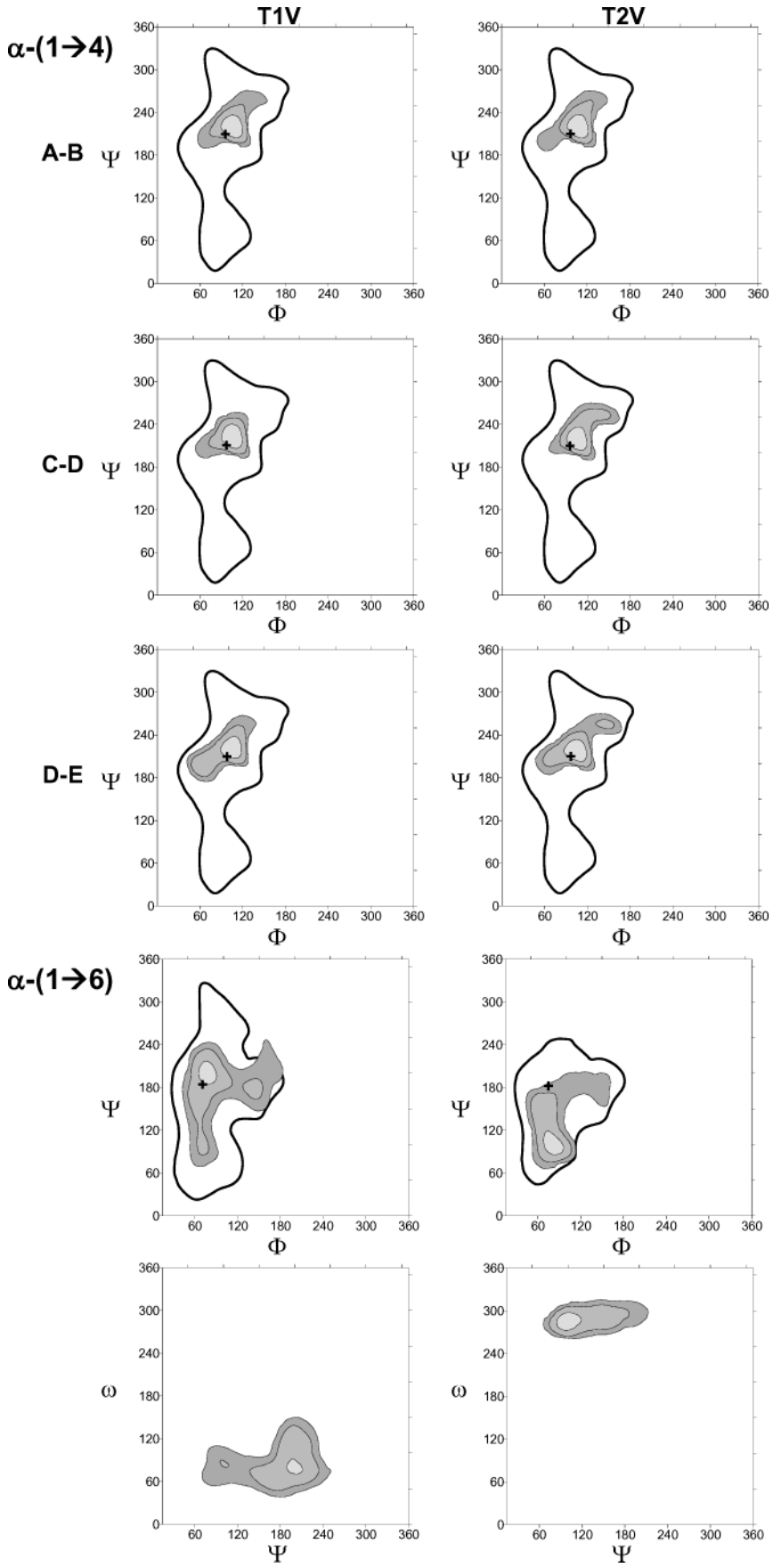

Figure 2. Population density map for the α-(1→4) and α-(1→6) linkages of the branched pentasaccharide in the two vacuum trajectories, T1v and T2v. Contours are drawn at (0.01, 0.001, and 0.0001) population levels. All figures have been superimposed on the outer contour of the MM3 energy maps of α-maltose (8 kcal·mol^{-1}) or α-isomaltose (6 kcal·mol^{-1}). The figures include the position of the global minimum (+) calculated in MM3.

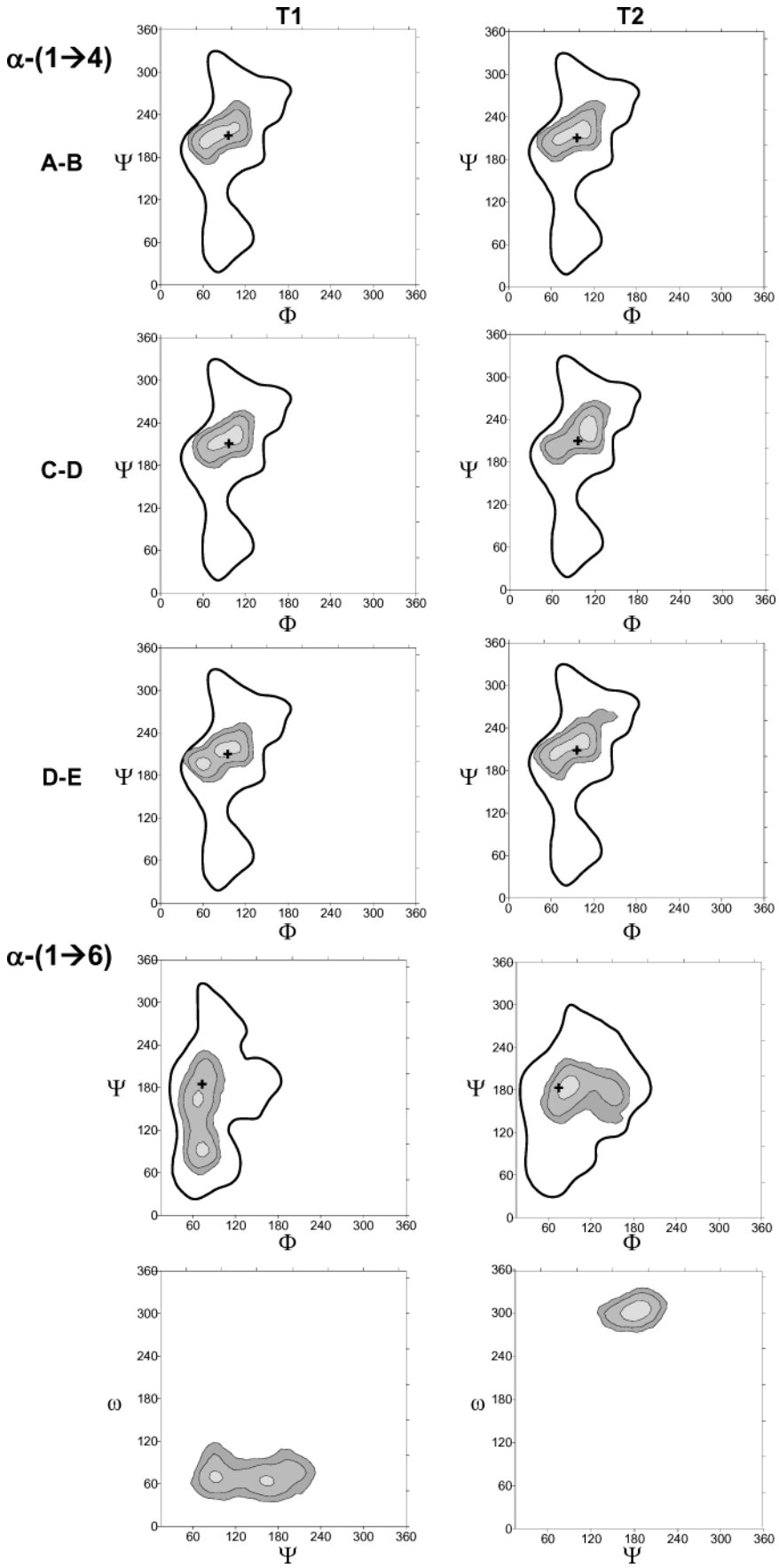

Figure 3. Population density map for the α-(1→4) and α-(1→6) linkages of the branched pentasaccharide in the two trajectories, T1 and T2, recorded in aqueous solution. Contours are drawn at (0.01, 0.001, and 0.0001) population levels. All figures have been superimposed on the outer contour of the MM3 energy maps of α-maltose (8 kcal·mol^{-1}) or α-isomaltose (6 kcal·mol^{-1}). The figures include the position of the global minimum (+) calculated in MM3.

Table 1. Conformation of the α-(1→6) Linkage in the Pentasaccharide Simulations Compared to the Proposed Starch Branch Point Conformations[50] and to a Few Crystal Structures

α-(1→6)	Φ	Ψ	ω
$T1_{(\Psi\sim180)}$	⟨67°⟩	⟨166°⟩	⟨65°⟩
$T1_{(\Psi\sim90)}$	⟨70°⟩	⟨91°⟩	⟨68°⟩
T2	⟨95°⟩	⟨179°⟩	⟨300°⟩
Starch "T1"[50]	60°	180°	30°
Starch "T2"[50]	77°	98°	298°
α-panose[47]	71°	165°	76°
melibiose·H_2O[51;52]	76°	186°	297°
raffinose·$5H_2O$[53]	72°	189°	297°
stachyose·$5H_2O$[54]	85°	188°	87°
	65°	185°	298°

Table 2. Chemical Shift and Coupling Constant Data at 500 MHz for ^{1}H and 125 MHz for ^{13}C NMR[a] of Methyl 6′-α-Maltosyl-α-maltotrioside at 5 °C

residue	H1	H2	H3	H4	H5	H6a,b
A and **C**	5.047 $J_{1,2} \approx 4$ (100.6)	3.234 (72.7)	3.351 (73.7) 3.354 (73.7)	3.073 (70.08) 3.056 (70.16)	3.392 (73.6) 3.417 (73.6)	3.40−3.59 (61.0−61.4)
B	4.642 $J_{1,2} = 4.0$ (99.6)	3.240 (72.1)	3.681 (74.2)	3.326 (78.01)	3.535 (71.2)	3.40−3.59 (61.0−61.4)
D	5.023 $J_{1,2} = 3.6$ (100.6)	3.287 (72.3)	3.637 (74.0)	3.335 (78.40)	3.693 (71.1)	3.522, 3.624 (68.03)
E	4.474 $J_{1,2} = 3.8$ (100.0)	3.258 (71.9)	3.594 (74.4)	3.285 (78.42)	3.442 (71.0)	3.40−3.59 (61.0−61.4)

[a] The $J_{1,2}$ values were measured in the 1D spectrum at 25 °C. All glucosyl residues displayed the expected cross-peak fine structure in the DQCOSY spectrum: $J_{2,3} \approx 10$ Hz, $J_{3,4} \approx 8$ Hz, and $J_{4,5} \approx 10$ Hz.

The geometry distribution of the branch point obtained from trajectory T2 appears relatively monodisperse, and the Ψ dihedral has a value around 180°. This geometry, which presents a parallel orientation of the α-(1→6) branch (D−B−A) with respect to the glucan backbone (E−D−C), differs only slightly from the one proposed by O'Sullivan and Pérez[50] for the α-(1→6) linkage (Starch "T2" in Table 1). It presents the two glucan short chains in the orientation required for formation of a double-helical structure, as visualized in Figure 4. The values reported for the α-(1→6) dihedrals by O'Sullivan and Pérez were $\Phi = 77°$, $\Psi = 98°$, and $\omega = 298°$, and in the T2 trajectory the average values of the corresponding dihedrals are $\langle\Phi\rangle = 95°$, $\langle\Psi\rangle = 179°$, and $\langle\omega\rangle = 300°$, in very good agreement with those observed in the crystal structures of different hydrated α-glucan compounds, such as melibiose·H_2O,[51,52] raffinose·$5H_2O$,[53] and stachyose·$5H_2O$[54] (see Table 1). The relatively large difference in the Ψ angle between the pentasaccharide and the proposed double-helical combination may be ascribed to constraints required by the helix formation. However, as visualized in Figure 4, the difference in the Ψ angle upon the overall branching geometry is not large, and it is quite possible that the proposed model is suboptimal due to the lack of experimental evidences in this combining region of the double-helical amylopectin fragment.

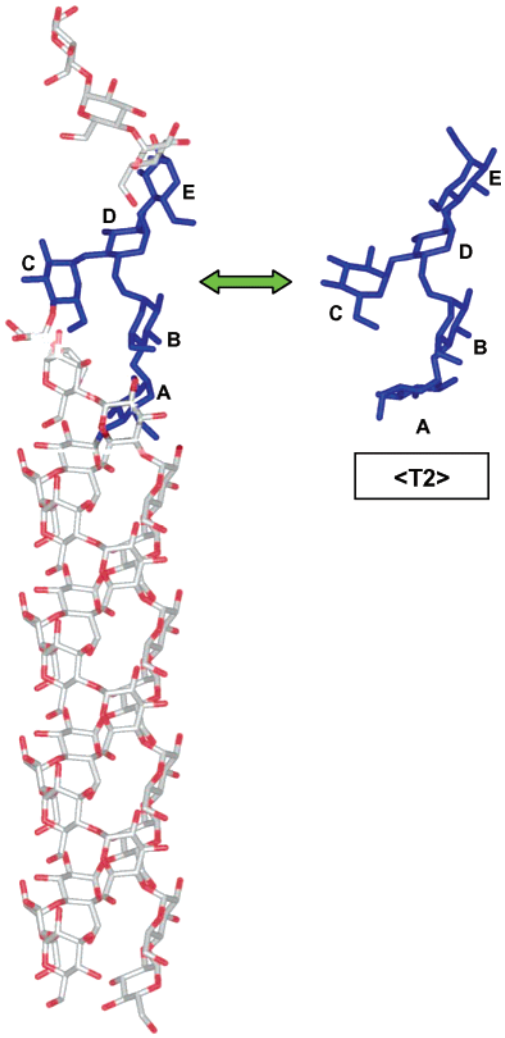

Figure 4. Optimized geometry of the amylosic double-helical fragments[50] constructed by the POLYSaccharide builder (POLYS)[64] and compared to the ensemble average conformation of the branched pentasaccharide obtained from trajectory T2.

The methyl group of the branched pentasaccharide was added in order to mimic an elongation of the glucoside backbone and to allow exact comparison between NMR experiments and molecular dynamics simulations. From an experimental viewpoint, in the absence of the methyl group mutarotation would occur, whereas in simple molecular dynamics simulations it is prohibited by the topology and harmonic bond potential used. As expected, the methyl group adopts a *gt* conformation throughout the trajectories, which is in agreement with the exo-anomeric effect. The *gg* conformation is never sampled due to strong steric conflicts between the methyl group and the axial hydrogens of the ring.

NMR Coupling Constants and NOE Experiments. As an independent check on the validity of the simulations, homo- and heteronuclear coupling constants, as well as translational and rotational coefficients, have been calculated from the trajectories and compared to those obtained from NMR experiments. Table 2 contains the 500 MHz ^{1}H and 125 MHz ^{13}C chemical shifts of a 13 mM solution of the pentasaccharide in D_2O at 5 °C.

(51) Kanters, J. A.; Roelofsen, G.; Doesburg, H. M.; Koops, T. *Acta Crystallogr., Sect. B: Struct. Sci.* **1976**, *32*, 2830−2837.
(52) Gress, M. E.; Jeffrey, G. A.; Rohrer, D. C. *Acta Crystallogr., Sect. B: Struct. Sci.* **1978**, *34*, 508−512.
(53) Berman, H. M. *Acta Crystallogr.* **1970**, *B26*, 290−299.
(54) Gilardi, R. D.; Flippen, J. L. *J. Am. Chem. Soc.* **1975**, *97*, 6264−6266.

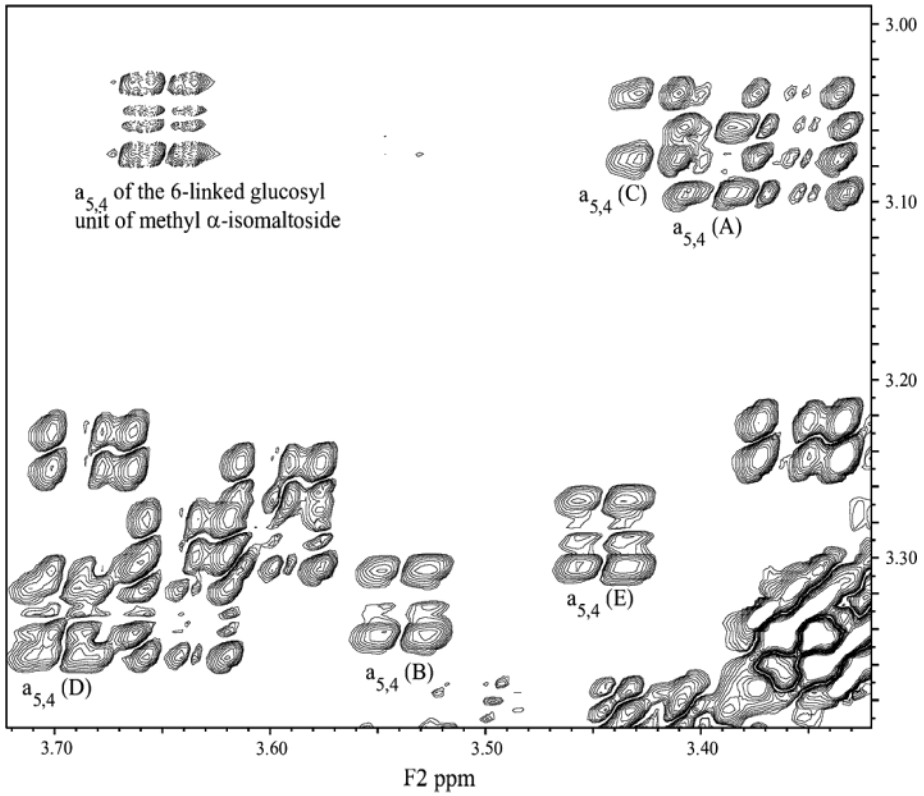

Figure 5. Expansion of the DQCOSY spectrum containing the H5/H4 cross-peaks, labeled $a_{5,4}$ (A−E), with the H5 frequency along F2. The $a_{5,4}$ cross-peak of the 6-linked glucose unit of methyl α-isomaltoside has been inserted into the upper left corner.

Chemical shift data for the pentasaccharide in $CDCl_3$ have been reported previously.[15] Small $^3J_{H5,H6a}$ and $^3J_{H5,H6b}$ coupling constants were determined for the terminal sugars (1.8 and 2.7 for A; 1.7 and 2.6 for C) in $CDCl_3$, pointing to dominant *gg* rotamer populations,[55] but the H5−H6a,b chemical shifts and vicinal coupling constants could not be determined for residues B, D, and E due to severe spectral crowding. In the study of the model disaccharides methyl α-maltoside and methyl α-isomaltoside[40], the $^3J_{H5,H6R}$ and $^3J_{H5,H6S}$ values (approximately 5 and 2 Hz for all four glucosyl residues) suggested roughly equal *gg* and *gt* populations of primary hydroxyl rotamers. The usual chemical shift order of the methylene protons (H6S and H6R resonating at low and high field, respectively) was reversed for the 6-linked glucosyl unit of methyl α-isomaltoside, as has been observed for residue D of the pentasaccharide in the present work.

The spectral dispersion of the DQCOSY spectrum in D_2O at 5 °C was satisfactory for the methine proton signals (only the methylene proton resonances displayed severe overlapping), and an expansion containing the H5/H4 cross-peaks, $a_{5,4}$ (A−E) with the H5 frequency along F2, is given in Figure 5, along with an insert of the $a_{5,4}$ cross-peak of the 6-linked glucose unit of methyl α-isomaltoside. The only pentasaccharide $a_{5,4}$ cross-peak showing further splitting of the anti-phase doublet due to the passive $^3J_{H5,H6R}$ coupling is the 1,4,6-trisubstitued residue D. Its fine structure is almost identical to that of the inserted $a_{5,4}$ cross-peak of the 6-linked glucose unit of methyl α-isomaltoside, pointing to about equal *gg* and *gt* rotamer populations for D. Inspection of the remaining $a_{5,4}$ cross-peaks in the DQCOSY spectrum suggests that the active H5/H4 couplings are analogous to the one that can be extracted from the insert ($^3J_{H5,H4}$ 10.1 Hz), but the passive $^3J_{H5,H6R}$ and $^3J_{H5,H6S}$ couplings are smaller for residues B, E, and especially A and C, in line with the data obtained in $CDCl_3$.[15] These experimental coupling constants indicate that the *gg* rotamer populations follow the order C ∼ A > E ∼ B > D.

Table 3. Measured and Calculated ^3J Coupling Constants (Hz) of Methyl 6′-α-Maltosyl-α-maltotrioside

^3J	exptl	T1	T2
$C_{4'}(B)-H_1(A)$	3−4[a]	3.39	0.99
$C_{4'}(D)-H_1(C)$	3−4[a]	4.21	1.30
$C_{4'}(E)-H_1(D)$	3.5	3.48	1.07
$C_{6'}(D)-H_1(B)$	4.1	1.18	1.31
$C_1(A)-H_{4'}(B)$		3.94	4.78
$C_1(C)-H_{4'}(D)$		4.30	4.10
$C_1(D)-H_{4'}(E)$		3.82	5.03
$C_1(B)-H_{6S'}(D)$		2.89	1.93
$C_1(B)-H_{6R'}(D)$		3.36	1.93
$H_5(D)-H_{6S}(D)$	<2[b]	1.67	1.98
$H_5(D)-H_{6R}(D)$	∼5[b]	9.52	0.55

[a] Overlapping. [b] From the DQCOSY spectrum.

To probe the conformational preferences of the various glycosidic linkages, homonuclear NOE experiments and accessible heteronuclear coupling constants across the α-(1→4) and α-(1→6) glycosidic linkages were measured. The ensemble average theoretical coupling constants are listed in Table 3. The soft pulses on carbon were not sufficiently selective to allow a precise measure of the $^3J_{C4',H1}$ and $^3J_{C1',H4}$ values, as the C4′ signals of the B, D, and E residues were excited simultaneously, leading to an antiphase doublet for $H1_D$ (3.5 Hz) and two overlapping antiphase doublets for $H1_A$ and $H1_C$ (3−4 Hz) (the passive H1/H2 couplings were suppressed with band-selective homo-decoupling at the H2 frequencies). The $^3J_{C6',H1}$ value of

(55) Bock, K.; Duus, J. Ø. *Carbohydr. Chem.* **1994**, *13*, 513−543.

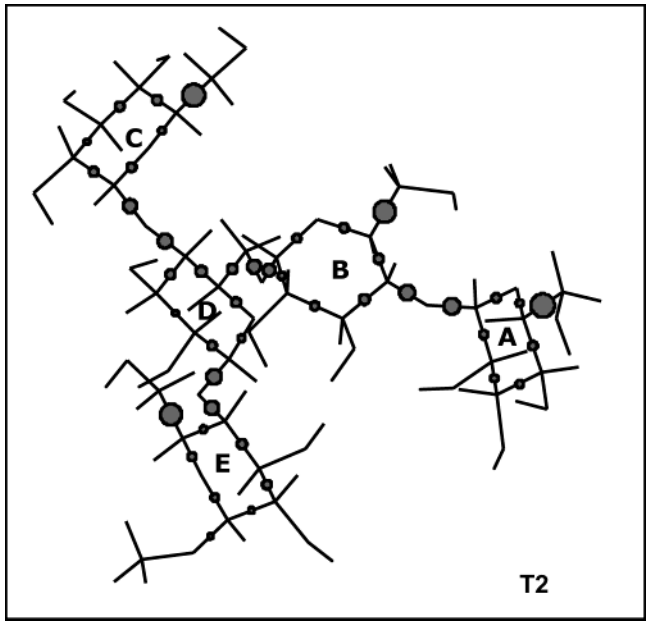

Figure 6. PCA dihedral model for T2. Logarithmic sum of the squared score values for a three-component model projected onto a drawing of the original branched pentasaccharide.

4.1 Hz could be measured more accurately and is slightly larger than the corresponding coupling constant in methyl α-isomaltoside (3.2 Hz).

The volumes of inter-residue NOESY cross-peaks (5 °C) were compared with the intra-residue H1/H2 cross-peak volumes that correspond to a ~2.5 Å distance in α-glucosyl residues. The following strong sequential interactions were observed: H1(A)/H4(B) and H1(C)/H4(D) overlapping (120% of the summed intraresidue H1/H2 cross-peak volumes), H1(D)/H4(E) and H1(D)/H2(D) strong but overlapping, H1(B)/H6S(D) and H1(B)/H6R(D) (60 and 20%, respectively, of H1(D)/H2(D)), and H1(E)/OCH_3 (50% of the H1(E)/H2(E) volume). However, these experimental data are predicted for both trajectories and do not allow discrimination between the different geometries of the α-(1→6) linkage obtained in the present work.

Exploratory Trajectory Analysis of Solute Flexibility. PCA was used to explore the branched pentasaccharide dihedral simulation time profiles. The analysis of trajectory T2 shows that components 1−3 explain 67.6, 89.6, and 96.6% of the cumulative variation in the original data in eq 2. This means that, after extracting three components, only 3.4% of the total variation is not described by the model. Other diagnostics also indicate that three components represent the correct underlying complexity for these data,[41] and henceforth we will focus on these first three factors. An overall impression of the model was obtained by summing the squared dihedral scores for components 1−3, yielding a parameter that can be interpreted in terms of quantitative flexibility indices of the bonds. Figure 6 shows the logarithmic value of the squared and summed dihedral scores for simulation T2, projected on an arbitrary structure of the branched pentasaccharide (logarithmic instead of original values are chosen to obtain a more comparative representation). When applied to the T1 trajectory, this analysis reveals a quite similar representation. The PCA results confirm the expectation that the exocyclic torsions show more flexibility (larger contour circles) than the more rigid torsions (smaller contour circles) within the ring structures. The glucosidic linkage bonds display a flexibility that is lower than the exocyclic torsions, but larger than any of the endocyclic torsions. Most importantly, the figure reveals that the α-(1→6) glycosidic linkage between glucose residues D and B exhibits significantly less flexibility than the α-(1→4) linkages. In particular, the ω dihedral exhibits much less flexibility than the Φ and Ψ dihedrals. In the starch pentasaccharide, which has a relatively spherical overall shape (i.e., the anisotropic ratio is <1.3), the variations in the heteronuclear Overhauser effects, η_{C-H}, will be qualitatively related to the so-called order parameters that represent the spatial restriction of motion for the C−H bond vectors (i.e., increased flexibility will result in reduced η values). On the basis of this criterion, comparison of the experimental η_{C-H} for C1 and C4 of residues B (1.1, 1.3), D (1.4, 1.6), and E (1.0, 0.9) corroborates reduced flexibility for the glycosidic linkages of the former residues.

Translational and Rotational Diffusion. The translational diffusion can be theoretically calculated using the Stokes−Einstein relation by calculating the center of mass mean-square displacement autocorrelation. Figure 7A shows the diffusion coefficient as a function of time, obtained using this approach. The plots have a characteristic backscatter maximum approximately 1 ps after the initial period of free movement. The translational diffusion coefficients calculated from the different trajectories in H_2O are in relatively good accordance with the experimental determination of $(2.16 \pm 0.03) \times 10^{-6}$ $cm^2 \cdot s^{-1}$ in D_2O using pulsed field gradient NMR experiments (taking into account the difference in viscosity, η_{D_2O}/η_{H_2O}, of 1.23 at 25 °C). The experimental value is analogous to those obtained for oligosaccharides of similar sizes [$(2.35-2.74) \times 10^{-6}$ $cm^2 \cdot s^{-1}$ for linear tetrasaccharides or a branched heptasaccharide with a tetrasaccharide backbone] found in a systematic study of diffusion coefficients of oligosaccharides as a function of size.[32]

The rotational diffusion, or the overall molecular tumbling time for the solute, can be estimated from the angular evolution of the solute dipole moment, as expressed by the autocorrelation function for the angular displacement of the dipole moment vector, and can be assessed from the global correlation time (τ_c), obtained from heteronuclear relaxation data[40,56] (Figure 7B). The average value of the methine heteronuclear NOE factor ($\eta_{CH} = 1.2$) was compared to the theoretical plot of η_{CH} versus τ_c for various motional models, which resulted in an approximate τ_c value of 3.4×10^{-10} s. The very small homonuclear NOEs at 25 °C corroborated that the rotational correlation time was close to the zero-crossing at 500 MHz ($\omega\tau_c \approx 1.12$ gives a value of 3.6×10^{-10} s).[57] Once more, the calculated values are in good agreement with the experimentally measured one.

Anisotropic Hydration. To gain detailed knowledge about the influence of water upon the preferred conformation of the branched pentasaccharide, we calculate first the number of close neighbor water molecules as a function of time. In the T1 trajectory, the average hydration number is calculated to be 40.1 and 10.3 for water oxygen distances less than 3.5 and 2.8 Å from the pentasaccharide oxygens, respectively. Almost identical values (40.2 and 10.2) are calculated for the T2 trajectory, showing the insensitivity of hydration numbers to conforma-

(56) Dais, P. *Adv. Carbohydr. Chem. Biochem.* **1995**, *51*, 63−131.
(57) Neuhaus, D.; Williamson, M. *The Nuclear Overhauser Effect in Structural and Conformational Analysis*; VCH Publishers: New York, 1989.

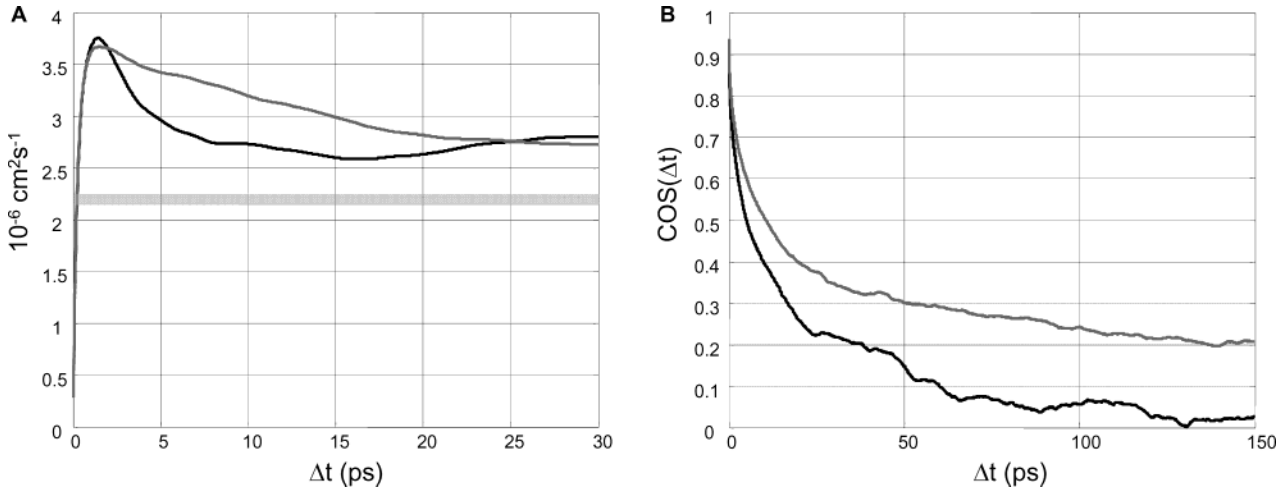

Figure 7. Calculated (A) translational and (B) rotational diffusion of the branched pentasaccharide from the two trajectories, T1 and T2. The thick horizontal gray line represents the experimental value measured in this work. The result calculated from the T1 trajectory is indicated with continuous black lines and the results from the T2 trajectory with continuous gray lines.

tional changes. The values for the pentasaccharide are approximately twice as high as those calculated for corresponding disaccharide subunits, methyl α-D-maltoside and methyl α-D-isomaltoside, which yielded values of approximately 20 and 5[40] using the same force field. Keeping in mind that the interaction energy of one glucose unit (α-D-glucopyranose) with one single water molecule (its crystalline hydratation water) is estimated by high-level *ab initio* methods to be at least 4.9 kcal/mol,[58,59] these results indicate that we have a significant loss of hydration energy, because the hydration number would ideally be proportional to the number of exposed solute hydroxyl oxygens. This result reflects a relatively nonflexible, compact structure of the branched pentasaccharide primarily induced by the 1,4,6-trisubstituted glucose residue, in good agreement with the principal component trajectory analysis.

The next step was to investigate the anisotropic hydration of the solute. Since radial pair distribution functions only carry hidden information on localized hydration sites, normalized two-dimensional radial pair distributions[60] were calculated for all possible shared water density sites (Os1···Ow···Os2), where Ow is the water oxygen and Os is solute oxygen. In these calculations, the likelihood of finding a water molecule in a well-defined local intersection area is compared and scaled to the likelihood of finding a bulk water molecule in the same local intersection area. Such calculations lead to water densities higher than bulk water density when structural or semistructural water molecules are present, and Table 4 shows the peak density of the most important interglycosidic water bridges found in the trajectories. As has been demonstrated in the case of α-maltose,[40,61] bridging water molecules between oxygens 1 O2 and 2 O3 compete with direct solute hydrogen bonds (not shown).

The most populated water bridge found in trajectory T1 corresponds to the situation where the two major families of conformations ($\Psi \approx 90°$ and $\Psi \approx 180°$) both accommodate a water bridge between O2(B) and O6(E). The maximum density of this shared water site was 2.0 times the bulk density (Figure 8), and the average residence time for a bridging water molecule was about 0.21 ps (the maximum residence time in the simulation was 9.18 ps). However, the water bridge is apparently in competition with a direct intramolecular hydrogen bond, as the distance O2(B)···O6(E) is less than 3.3 Å during 60% of the time (19% if the distance Os···Os ≤ 2.8 Å). Due to the cooperative effects of hydrogen bonding and the water bridge, the average geometry of the branch point is relatively restricted and exhibits an orthogonal orientation of the α-(1→6) branch (D−B−A) with respect to the glucan backbone (E−D−C), which differs from the antiparallel arrangement found in a vacuum.

Table 4. Peak Water Densities of the 2D Pair Distribution Functions Defining Statistical Bridging Waters in the "Pocket" Defined by Two Solute Oxygen Atoms[a]

	T1	T2		T1	T2
O2(A)−O3(B)	1.6	1.9	O2(B)−O6(E)	2.0	−
O6(A)−O6(B)	1.0	2.7	O6(B)−O6(C)	−	1.5
O5(B)−O6(C)	−	−	O2(B)−O3(E)	−	−
O2(C)−O3(D)	1.3	−	O1(B)−O6(E)	−	−
O2(D)−O3(E)	1.0	1.5	O4(A)−O6(B)	−	−
O2(B)−O5(D)	−	8.5			

[a] A value of 1.0 indicates bulk water density and "−" indicates that no shared water position is possible.

In trajectory T2, the major conformation adopts a parallel orientation of the α-(1→6) branch (D−B−A) with respect to the glucan backbone (E−D−C). In this case, a most significant water bridge was also found between oxygens O-2(B) and O-5(D), with an anisotropic water density of 8.5 (Figure 8), which is unusually high for the force field used[40] but similar in magnitude to the shared water between O-2g and O-1f reported for sucrose.[60] In the pentasaccharide, the water bridge between O-2(B) and O-5(D) is present about 73% of the time, having maximum and average residence times of 18.36 and 0.57 ps, respectively. The average distance O-2(B)···O-5(D) was 4.49 Å, ranging from 5.49 to 2.62 Å. The existence of this water bridge probably explains the reduced flexibility of the branch point of the pentasaccharide when compared to the observations made for the tetrasaccharide 6″-α-D-glucopyranosyl-maltotri-

(58) Hemmingsen, L.; Madsen, D. E.; Esbensen, A. L.; Olsen, L.; Engelsen, S. B. *Carbohydr. Res.* **2004**, *339*, 937−948.
(59) Momany, F. A.; Appell, M.; Strati, G.; Willett, J. L. *Carbohydr. Res.* **2004**, *339*, 553−567.
(60) Andersson, C. A.; Engelsen, S. B. *J. Mol. Graph. Modell.* **1999**, *17*, 101−105.
(61) Brady, J. W.; Schmidt, R. K. *J. Phys. Chem.* **1993**, *97*, 958−966.

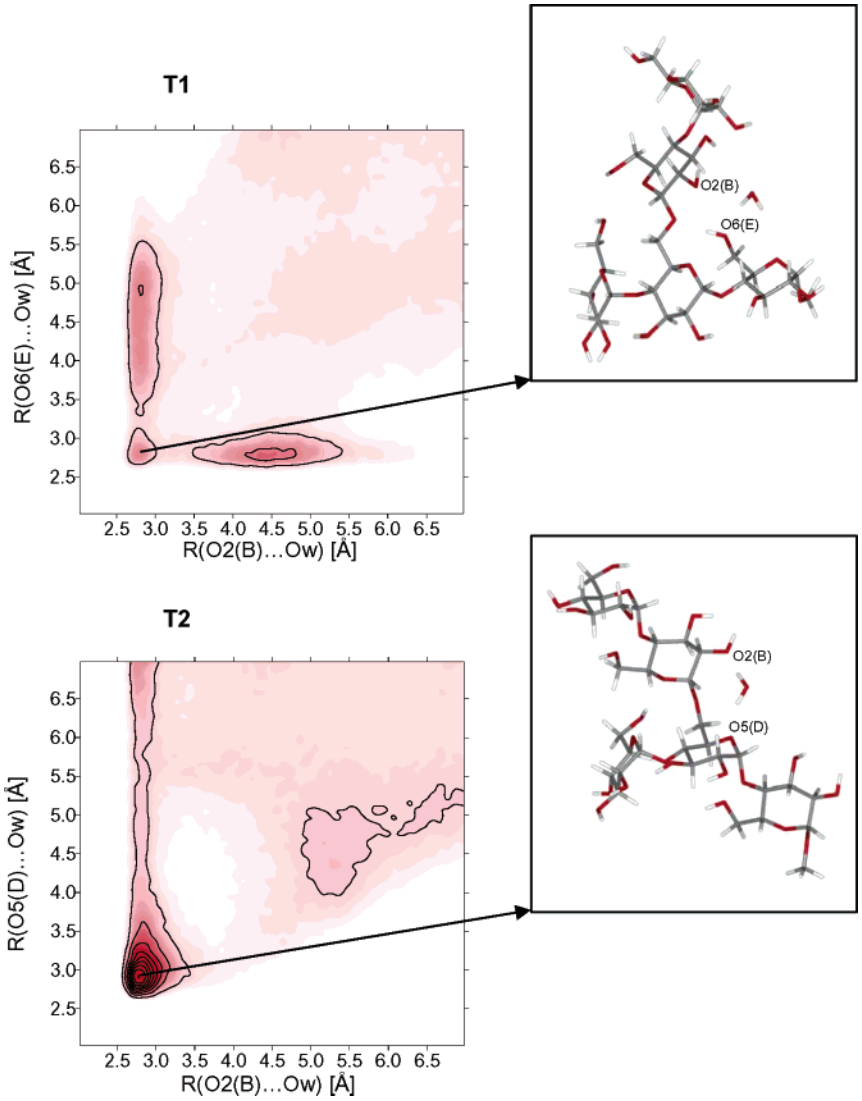

Figure 8. Two-dimensional radial pair distribution functions of different bridging water situations found in the four trajectories. Contour levels are drawn at 0.96, 2.0, 3.0, 4.0, 5.0, 6.0, and 7.0 times the bulk water density.

ose.[19] This result is highly interesting, as it indicates that extending the α-(1→6) branch (D−B−A) by one glucose unit (A) paves the way for a water bridge between O-2(B) and O-5(D) that "locks" the branch point structure into a conformation that ultimately will lead to double-helical formation between the two branches (E)−D−C and D−B−A. Moreover, it suggests that this water molecule should be present as structural water in the limiting region of the amylopectin crystalline region. However, thus far, no such evidence has been reported, perhaps because such structural water molecules are outnumbered (beyond X-ray detection limits) by the structural waters in the double-helical regions.

Conclusions

The α-glucan pentasaccharide is the best starch branching model that has been synthesized and characterized thus far, and for the first time we have results that indicate nonsteric elongation and branching of the amylopectin molecule in an aqueous environment. The results in this study all suggest that the conformational flexibility of the α-(1→6) branch point in water is low. This was first indicated by explorative PCA of the molecular dynamics trajectories, subsequently explained by detailed and directional hydration features, and finally corroborated by very good agreement between the theoretical molecular dynamics models and NMR spectroscopy. The apparent rigidity of the branch point could be explained by the presence of localized water densities or water bridges across the branch point that have a determining influence on the preferred conformation. Most significant is the high water density found around the α-(1→6) linkage in the T2 trajectory. In this trajectory, the α-(1→6) branch (D−B−A) adopts a parallel arrangement with respect to the glucan backbone (E−D−C) suitable for the formation of the amylopectin double helices. The geometry is similar to the one suggested by O'Sullivan and Pérez[50] for the α-(1→6) region that unites the two short-chain glucans into a double-helical structure. Moreover, the second family of conformations T1 that was observed in the molecular dynamics simulations, with a nearly orthogonal branching pattern, exhibits an average geometry that is similar to the branching structure interconnecting two double helices.[50]

It is important to underline that the results obtained in this work differ from those of previous studies of the amylopectin branch point geometry, including a recent study of the α-(1→6)

linkage behavior in the model compound 6″-α-D-glucopyranosyl-maltotriose[19] which was examined using largely the same methods. In the tetrasaccharide case, it was found that the three-bond α-(1→6) linkage was highly flexible. In particular, the authors observe additional important transitions in the Ψ dihedral when compared to the α-(1→6) linkage in isomaltose that were explained by assuming that the additional residues increase flexibility. Our results on the pentasaccharide strongly suggest that the prolongation of the α-(1→6) branching chain B by one additional glucose residue B−A can lead to a relatively rigid overall conformation that accommodates a highly significant water bridge in the vicinity of the α-(1→6) linkage and which, in our view, is the likely physical explanation for the alignment of two amylopectin strands in a parallel double-helical fashion.

While our results point toward a highly probable nonsteric elongation and branching of the amylopectin molecule in an aqueous environment, synthesis and thorough theoretical investigations of larger amylopectin fragments are required to establish this structural behavior. Using the short-chain model glucans, the role of α-(1→6) linkages in the so-called amorphous regions cannot be fully understood. Thus, larger and more complex systems need to be characterized. The hydroxyl protons of carbohydrates have been used as conformational probes of inter-residue hydrogen bonds in supercooled water[62] and in acetone/water solvent mixtures at a low temperature.[63] However, the relevance of behavior exhibited under such experimental conditions to our simulated data is questionable. Nevertheless, application of these approaches to model starch systems will be considered in future work.

Acknowledgment. The Centre for Advanced Food Studies, the Danish National Research Foundation, and the Scandinavian Øforsk program ØSP are acknowledged for financial support. Gilda Kischinovsky is thanked for assistance with the manuscript. We would like to thank anonymous reviewers for valuable corrections and additions to the manuscript.

JA048622Y

(62) Sheng, S. Q.; van Halbeek, H. *Biochem. Biophys. Res. Commun.* **1995**, *215*, 504−510.
(63) Bekiroglu, S.; Kenne, L.; Sandström, C. *J. Org. Chem.* **2003**, *68*, 1671−1678.
(64) Engelsen, S. B.; Cros, S.; Mackie, W.; Pérez, S. *Biopolymers* **1996**, *39*, 417−433.